Sensors and Materials, Vol. 34, No. 6 (2022) 2155–2160
MYU Tokyo

S & M 2962

Numerical Modeling of Guided Mode for Negative Curvature Hollow-core Fibers

Jung-Sheng Chiang,* Min-Yu Tsai, and Nai-Hsiang Sun

I-Shou University, 1, Sec. 1, Syuecheng Rd., Dashu District, Kaohsiung City 84001, Taiwan, R.O.C.

(Received December 6, 2021; accepted April 20, 2022)

Keywords: negative curvature hollow-core fiber, vector boundary element method, photonic crystal fiber

In this paper, we analyze the guided-mode properties of negative curvature hollow-core fibers (NCHCFs) using a new algorithm derived from the vector boundary element method (VBEM). We present a numerical analysis of NCHCFs for core-diameter ratios from 0.46 to 0.64 and eight-capillary cladding. It is found that the guided mode is effectively limited to within the hollow core when the core-diameter ratio is 0.51 to 0.62, enabling the core to confine the transmission power without leakage.

1. Introduction

Negative curvature hollow-core fibers (NCHCFs) are composed of a hollow core with multiple capillaries periodically arranged around the core to form a photonic crystal fiber.[1–4] These novel photonic crystal fibers characterized by the core wall's inverted curvature enable light transmission in a hollow core with low-refractive-index media such as air and vacuum. The guidance mechanism of NCHCFs is based on the anti-resonance effect in glass core walls that act as a Fabry–Perot cavity, and the anti-resonance effect is strengthened through inhibition of the coupling effect to reduce the transmission attenuation and enhance the operational bandwidth.[5–7] A guiding light in a large hollow air-filled core endows NCHCFs with the favorable properties of high power transmission, ultralow dispersion, a large bandwidth, and a simple structure.[8–11] In 2020,[12] we used a combination of an NCHCF and a gold-plated graded-index fiber to fabricate a hollow-core photonic crystal fiber sensor and we analyzed the sensing properties of the NCHCF sensor by measurement. We also modeled a surface-plasmon photonic crystal fiber (PCF)-based sensor in a hollow-core photonic crystal fiber.[13] It was found that the design of the hollow-core photonic crystal fiber considerably affects the sensor's performance. Therefore, understanding NCHCFs will be important for designing hollow-core photonic crystal fiber sensors.

NCHCFs with significantly lower transmission loss than other hollow-core photonic crystal fibers, such as photonic band-gap fibers and Kagome fibers, and a simple cladding structure characterized by very low coupling of the core and cladding modes have been proposed.[14] In 2011, Pryamikov *et al.* proposed an NCHCF with negative curvature of the core–cladding

*Corresponding author: e-mail: cjs@isu.edu.tw
https://doi.org/10.18494/SAM3806

ISSN 0914-4935

interface in the waveguide regime.[15] In 2015, Günendi *et al.* demonstrated an NCHCF with six-capillary cladding engineered to strongly suppress higher-order modes to realize a broadband single mode.[16] In 2016, Yu *et al.* experimentally studied the low-loss single-mode performance of NCHCFs with seven- and eight-capillary cladding.[17] A promising NCHCF for sensing applications with an all-fiber interferometer based on an NCHCF structure was first proposed in 2020 by Liu *et al.*[18]

In this work, we propose a new algorithm for the vector boundary element method (VBEM) to model and analyze the guided-mode properties of NCHCFs with core-diameter ratios from 0.46 to 0.64 and eight-capillary cladding.

2. Simulation Method

In this study, a new vectorial algorithm is derived from the VBEM[19–22] for modeling guided modes in an NCHCF by simply solving the propagation constants corresponding to the supported modes of the NCHCF structure. To our knowledge, this is the first time an approach based on the boundary element method has been used for a hollow-core photonic crystal fiber.

Two homogeneous regions describe a hollow-core fiber: the air of the fiber core and the capillaries. We denote E as an arbitrary function in the rectangular coordinate system that is the solution of the Helmholtz equation in each region as follows:[22]

$$\nabla_t^2 E(\vec{r}) + k^2 E(\vec{r}) = 0, \tag{1}$$

where ∇_t^2 represents the Laplacian operator in a transverse plane. The differential equation Eq. (1) is converted to the following integral equation by using Green's identities:[22]

$$E(\vec{r}) = \oint_{\Gamma} \left(E(\vec{r}') \frac{dG(k,\vec{r},\vec{r}')}{dn} - G(k,\vec{r},\vec{r}') \frac{dE(\vec{r}')}{dn} \right) d\vec{r}'. \tag{2}$$

The 2D Green's function G takes the form $G = (-j/4) H_0^{(2)}(k|\vec{r} - \vec{r}'|)$, where $H_0^{(2)}$ is the zeroth Hankel function of the second kind. In Eq. (2), Γ denotes the boundary contour of two homogeneous regions and d/dn indicates a normal inward derivative. If Γ is sufficiently smooth to calculate points approaching the boundary, then Eq. (2) becomes

$$\frac{1}{2} E(\vec{r}) = P\int_{\Gamma} \left(E(\vec{r}') \frac{dG(k,\vec{r},\vec{r}')}{dn} - G(k,\vec{r},\vec{r}') \frac{dE(\vec{r}')}{dn} \right) d\vec{r}', \tag{3}$$

where $P\int$ denotes the Cauchy principal value integral with the singularity at the point $\vec{r} = \vec{r}'$ removed.[22]

3. Modeling and Discussion

In our numerical analysis of the guiding modes for the NCHCF, we calculate the propagation constants and effective index of the fundamental core modes of the hollow core with multiple

capillaries periodically arranged. As the NCHCF relies on a combination of anti-resonance and inhibition of the coupling effect, the higher-order modes are coupled to the cladding and are removed from the core. Therefore, the fundamental core mode can be propagated and confined in the hollow core with very low loss.

Here, we apply an NCHCF consisting of an eight-capillary cladding structure with circular capillaries to demonstrate the numerical results of our approach. A schematic cross section of the NCHCF with the eight-capillary cladding structure is shown in Fig. 1(a); the core is air, for which n_a is 1.0, and d_{core} is the core diameter in the fiber. The refractive index n_s of the capillary of the cladding is 1.45, and d_{in} and d_{out} are the inner and outer diameters of the capillary, respectively. Figure 1(b) shows the field distribution of the eight-capillary cladding structure of the NCHCF when the core-diameter ratio (d_{core}/D) is 0.51.

Figure 2 shows the effective index of the NCHCF versus the normalized wavelength for d_{core}/D of 0.46, 0.51, and 0.56. From this diagram, as d_{core}/D increases, the effective index (n_{eff}) increases accordingly. The transmission power of the NCHCF is strongly related to the propagation constant and effective index. Consequently, an NCHCF with a higher d_{core}/D has greater transmission power.

Figure 3 shows the guided-mode properties of NCHCFs having d_{core}/D from 0.46 to 0.64. We find that the guided mode is effectively limited to within the core when d_{core}/D is 0.51 to 0.62 for the eight-capillary cladding. The core of the NCHCF combines with the capillaries to form a resonance region. When d_{core}/D is too small, power leaks into the cladding because the negative curvature arc is short. In contrast, when d_{core}/D is too large, the anti-resonant effect is broken and the power also leaks. For d_{core}/D from 0.51 to 0.62, the transmission power can be confined to the core without leakage.

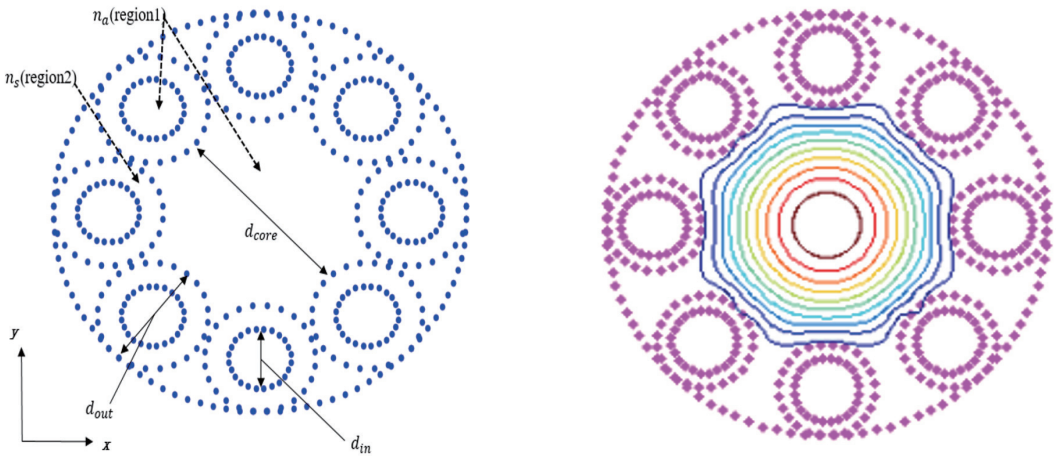

(a) (b)

Fig. 1. (Color online) (a) Schematic cross section of the NCHCF with an eight-capillary cladding structure; (b) field distribution of the NCHCF.

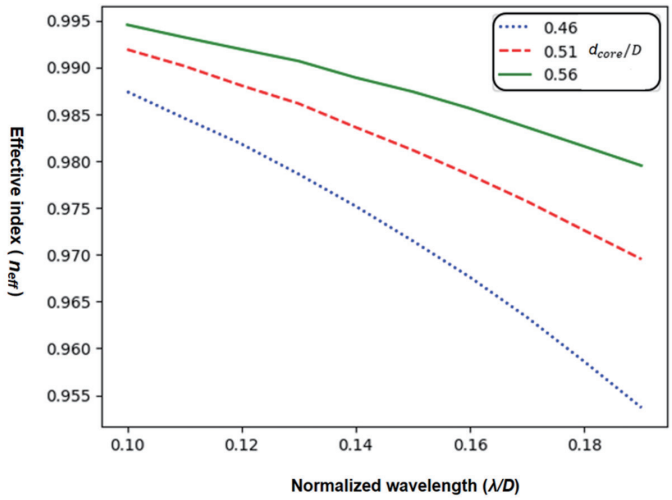

Fig. 2. (Color online) Effective index of NCHCF versus normalized wavelength for d_{core}/D = 0.46, 0.51, and 0.56.

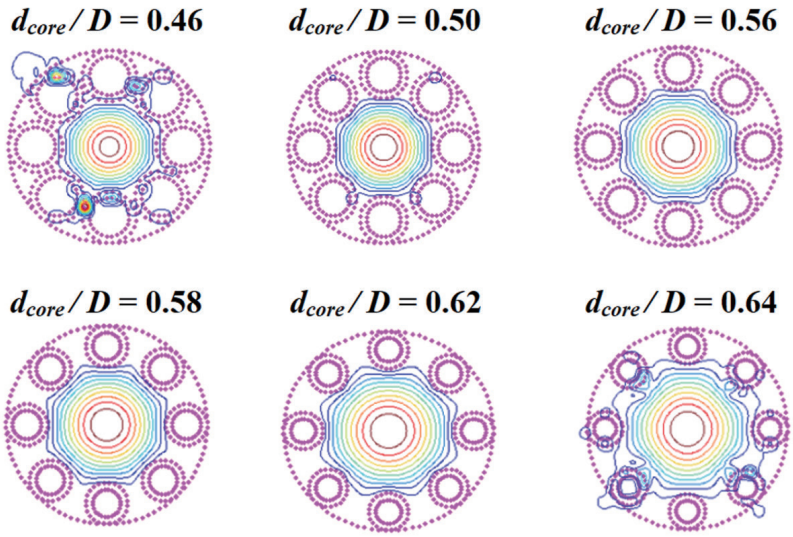

Fig. 3. (Color online) Field distributions of NCHCFs with d_{core}/D of 0.46 to 0.64.

4. Conclusions

In this work, we analyzed the guided-mode properties of NCHCFs using a new algorithm derived from the VBEM. We proposed an NCHCF with a simple cladding structure characterized by very low coupling of the core and cladding modes. This NCHCF has significantly lower

transmission loss than a photonic band-gap filter and a Kagome filter. We performed a numerical analysis of NCHCFs for core-diameter ratios (d_{core}/D) from 0.46 to 0.64 and eight-capillary cladding. When d_{core}/D is too small, the power leaks into the cladding because the negative curvature arc is short. In contrast, when d_{core}/D is too large, the anti-resonant effect is broken and the power also leaks. In the case of d_{core}/D from 0.51 to 0.62, the transmission power can be confined to the core without leakage.

Acknowledgments

This work was supported by the Ministry of Science and Technology, Taiwan, R.O.C., under Grants MOST-108-2221-E-214-030, MOST-108-2221-E-214-029-MY2, and MOST-110-2221-E-214-018, and the I-Shou University Grants ISU-108-01-01A and ISU-110-01-01A.

References

1 L. Vincetti and V. Setti: Opt. Express **18** (2010) 23133. https://doi.org/10.1364/OE.18.023133
2 W. Belardi and J. Knight: Opt. Lett. **39** (2014) 1853. https://doi.org/10.1364/OL.39.001853
3 M. Popenda, H. Stawska, L. Mazur, K. Jakubowski, A. Kosolapov, A. Kolyadin, and E. Bereś-Pawlik: Sensors **17** (2017) 2278. https://doi.org/10.3390/s17102278
4 I. Ankan, M. Mollah, J. Sultana, and M. Islam: Appl. Opt. **59** (2020) 8519. https://doi.org/10.1364/AO.395914
5 R. Carter, W. MacPherson, P. Jaworski, F. Yu, R. Beck, J. Shephard, and D. Hand: Opt. Eng. **55** (2016) 116106. https://doi.org/10.1117/1.OE.55.11.116106
6 M. Butt, S. Khonina, and N. Kazanskiy: J. Mod. Opt. **66** (2019) 1172. https://doi.org/10.1080/09500340.2019.1609613
7 W. Zheng, Y. Qin, O. Xu, M. Xiang, D. Peng, S. Fu, and J. Li: Opt. Express **29** (2021) 24182. https://doi.org/10.1364/OE.434015
8 P. Jaworski, F. Yu, R. Maier, J. Wadsworth, J. Knight, J. Shephard, and P. Hand: Opt. Express **21** (2013) 22742. https://doi.org/10.1364/OE.21.022742
9 J. Shephard, A. Urich, R. Carter, P. Jaworski, R. Maier, W. Belardi, F. Yu, J. Wadsworth, J. Knight, and P. Hand: Front. Phys. **3** (2015) 8498. https://doi.org/10.3389/fphy.2015.00024
10 F. Meng, B. Liu, Y. Li, C. Wang, and M. Hu: IEEE Photonics J. **9** (2017) 1. https://doi.org/10.1109/JPHOT.2016.2639004
11 C. Wei, R. Weiblen, C. Menyuk, and J. Hu: Adv. Opt. Photonics **9** (2017) 504. https://doi.org/10.1364/AOP.9.000504
12 J. Chiang, T. Chin, J. Lai, J. Syu, and N. Sun: Proc. 2020 Optics & Photonics Taiwan Int. Conf. (OPTIC, 2020) 269. https://optic2020.conf.tw/site/order/1350/SessionDetail.aspx?sid=1350&lang=en&snid=E
13 J. Chiang, J. Shie, W. Wang, and N. Sun: Proc. 2017 IEEE Opto-Electronics and Communications Conf. (IEEE, 2017) 1–2. https://doi.org/10.1109/OECC.2017.8114835
14 F. Yu and J. Knight: IEEE J. Quantum Elec. **22** (2016) 146. https://doi.org/10.1109/JSTQE.2015.2473140
15 A. Pryamikov, A. Biriukov, A. Kosolapov, V. Plotnichenko, S. Semjonov, and E. Dianov: Opt. Express **19** (2011) 1441. https://doi.org/10.1364/OE.19.001441
16 M. Günendi, P. Uebel, M. Frosz, and P. Russell: arXiv **1448** (2015) 6747. https://doi.org/10.48550/arXiv.1508.06747
17 F. Yu, M. Xu, and J. Knight: Opt. Express **24** (2016) 12969. https://doi.org/10.1364/OE.24.012969
18 D. Liu, W. Li, Q. Wu, H. Zhao, F. Ling, K. Tian, C. Shen, F. Wei, W. Han, G. Farrell, Y. Semenova, and P. Wang: Sensors **20** (2020) 4763. https://doi.org/10.3390/s20174763
19 T. Wu, J. Chiang, and C. Chao: IEEE Photon. Technol. Lett. **16** (2004) 1492. https://doi.org/10.1109/LPT.2004.827416
20 J. Chiang and T. Wu: Opt. Commun. **258** (2006) 170. https://doi.org/10.1016/j.optcom.2005.08008
21 J. Chiang, N. Sun, S. Lin, and W. Liu: J. Light. Technol. **28** (2009) 707. https://doi.org/10.1109/JLT.2009.2036945
22 J. Chiang: Crystals **8** (2018) 177. https://doi.org/10.3390/cryst8040177

About the Authors

Jung-Sheng Chiang received his B.S. degree in telecommunication engineering from National Chiao Tung University, Hsinchu, Taiwan, in 1995, his M.S. degree in space science from National Central University, Chungli, Taiwan, in 1999, and his Ph.D. degree in electrical engineering from National Sun Yat-sen University, Kaohsiung, Taiwan, in 2006. He is currently a professor of electrical engineering at I-Shou University, Kaohsiung, Taiwan. His research interests are in photonic crystal fibers, waveguide and optical fiber devices, plasmonics, and photonic crystal devices. (cjs@isu.edu.tw)

Min-Yu Tsai received his B.S. and M.S. degrees from I-Shou University, Kaohsiung, Taiwan, in 2006 and 2009, respectively. He is currently studying for a Ph.D. degree in electrical engineering at I-Shou University. His research interests are in the numerical modeling of dielectric waveguides. (isu10401002d@cloud.isu.edu.tw)

Nai-Hsiang Sun received his B.S. degree in electronic engineering from Chung Yuan Christian University, Chungli, Taiwan, in 1984, his M.S. degree in electrical engineering from National Cheng Kung University, Tainan, Taiwan, in 1986, and his Ph.D. degree in electrical engineering from Southern Methodist University, Dallas, TX, in 1997. Since 2010, he has been a professor at I-Shou University. His research interests are in periodic dielectric waveguides, fiber gratings, and numerical modeling of semiconductor lasers. (snh@isu.edu.tw)